Journal of Rock Mechanics and Geotechnical Engineering 18 (2026) 3819–3831

Contents lists available at ScienceDirect

Journal of Rock Mechanics and Geotechnical Engineering

journal homepage: www.jrmge.cn

Technical Note

Effectiveness of large-diameter combined tip-and-side post-grouted piles in deep fine sand layers: A field test study

Zhihui Wan [a,*], Zilong Guo [a], Guoliang Dai [b], Feng Zhou [a]

[a] College of Transportation Engineering, Nanjing Tech University, Nanjing, 211816, China
[b] School of Civil Engineering, Southeast University, Nanjing, 211189, China

ARTICLE INFO

Article history:
Received 3 March 2025
Received in revised form
3 July 2025
Accepted 17 July 2025
Available online 3 September 2025

Keywords:
Bored pile
Combined post-grouting
Static load test
Core drilling test
Standard penetration test (SPT)
Deep fine sand layer

ABSTRACT

This study investigates the effectiveness of combined tip-and-side post-grouting on large-diameter bored piles in deep fine sand layers. Field tests were conducted on nine piles for the Shishou Yangtze River Highway Bridge project. A detailed comparison of pile performance pre- and post-grouting assessed the technique's influence on ultimate bearing capacity and side resistance. The distribution and effectiveness of the cement grout were analysed using core drilling and the standard penetration test (SPT). An equation correlating post-grouting side resistance with the pre-grouting SPT index (N_{SPT}) was established. Results demonstrate a substantial improvement in pile bearing capacity after grouting. Ultimate bearing capacity increased by 76 %–152 % after grouting. Longer piles on the main bridge exhibited more pronounced enhancement, achieving ultimate capacities 145 %–206 % higher than those of the shorter approach bridge piles. This is attributed to the greater total cement volume applied along their sides. Critically, combined grouting outperformed side-only grouting, enhancing both side and tip resistance. Core drilling confirmed the spread of cement grout around the piles, confirming the method's effectiveness. SPT results indicated significant increases in the soil N_{SPT} adjacent to the piles following grouting. These findings provide directly applicable data for designing the bridge pile foundations and offer essential guidance for comparable projects in deep fine sand layers.

1. Introduction

The post-grouting technique is widely employed in various engineering projects, including skyscrapers, expansive bridges, high-speed rail systems, and offshore constructions, due to its ability to substantially enhance pile load-bearing capacity and reduce subsidence. Although pile tip grouting is a long-established and successful technique, side grouting for piles was implemented later. Gouvenot and Gabaix (1975) first reported field tests on six full-length steel piles subjected to side grouting, with three piles surrounded by sandy soil and the other three surrounded by clay soil, demonstrating that grouted steel piles exhibited 2–3 times greater bearing capacity than ungrouted counterparts under identical conditions. Subsequently, numerous researchers investigated the application of pile side post-grouting. Their research found that this method dramatically enhanced the synergy between the piles and the adjacent soil, increased side resistance, and, as a result, led to rapid advances in both its practical use and technological progress within the discipline (Littlechild et al., 1998; Nguyen and Fellenius, 2015). Recently, the construction industry has increasingly adopted combined tip-and-side post-grouting techniques to enhance the bored piles' bearing. This method has gained particular traction in large-scale infrastructure projects, such as bridge construction and offshore wind energy installations, where its effectiveness in significantly enhancing bearing performance has been widely recognized (Zhang et al., 2021; Gong et al., 2023; Liu et al., 2023; Wan et al., 2024).

Post-grouting constitutes an underground concealed operation, where the effectiveness of grouting is critical to the success of the entire project. Nevertheless, the inherently complex nature of grouting and the various influencing factors complicate precise impact assessment. Current assessment methodologies for post-grouting efficacy primarily include static load tests, core drilling

* Corresponding author.
E-mail address: wanzhihui@njtech.edu.cn (Z. Wan).
Peer review under responsibility of Institute of Rock and Soil Mechanics, Chinese Academy of Sciences.

https://doi.org/10.1016/j.jrmge.2025.07.004

tests, and standard penetration test (SPT). Among these, static load tests provide the most direct and reliable method for evaluating pile foundation load-bearing capacity pre- and post-grouting. Ma et al. (2021) investigated the impact of pile tip post-grouting on bored piles using static load tests on six test piles. To precisely map grout spread and quantify soil strengthening, core drilling tests and SPT have been commonly employed. Lin et al. (2000) also investigated the effects of post-grouting at pile bases, using core drilling to evaluate three different grouting techniques. Ho (2003) attempted to correlate the pile's side resistance, both before and after the grout job, to the SPT index, to determine the most effective post-grouting method down at the pile's tip. Notably, current studies primarily focus on evaluating pile tip post-grouting, with limited attention given to the effectiveness of combined tip-and-side grouting techniques. Hence, there is a critical need to investigate evaluation methodologies for assessing the effectiveness of combined grouting. Among these evaluation methods, SPT is widely applied in various engineering practices owing to its simplicity of equipment and ease of use. However, assessing pile foundation bearing capacity in real-world engineering is complex. Several approaches have been proposed to determine pile foundation bearing capacity directly using the SPT index (Horiguchi and Karkee, 1995; Homma, 2014; Huynh et al., 2022). However, current methods emphasize total pile foundation bearing capacity, neglecting the calculation of depth-dependent side resistance. Especially in post-grouted piles, variations in side resistance at specific depths reflect the effectiveness of grouting. Therefore, analysing the correlation between the SPT index and depth-dependent side resistance in post-grouted piles is essential.

This research investigated the impact of combined post-grouting on the load-bearing performance of large-diameter bored piles, based on a comprehensive analysis of in-situ static load tests conducted on nine piles for the Shishou Yangtze River Highway Bridge Project. The study meticulously examined and compared the outcomes of static load tests conducted on bored piles both pre- and post-grouting. It also investigated the influence of pile length on foundation bearing capacity and the role of cement quantity on the efficacy of the combined grouting technique. To evaluate the spread of cement grout along the pile, core drilling tests were conducted, offering insights into the effectiveness of the post-grouting method for ultra-long pile foundations in bridge construction. Field SPT was also utilized to measure the impact of grouting by comparing N_{SPT} before and after the process. Moreover, the correlation between side resistance and the N_{SPT} is established, accompanied by a predictive formula to estimate post-grouting side resistance distribution based on the pre-grouting SPT index. This approach serves as a valuable benchmark for future projects, particularly in fine sand layers, supporting informed decision-making in later stages of development.

2. Project background

2.1. Project overview

The Shishou Yangtze River Highway Bridge, depicted in Fig. 1, forms the pivotal structure for the Qianjiang-Shishou Expressway's Yangtze crossing in Hubei Province. The bridge is an engineering feat, showcasing remarkable technical sophistication. The centrepiece of the bridge features an 820-m double-tower, single-side hybrid girder cable-stayed design for its main span, arranged in a sequence of ($2 \times 75 + 80+820 + 300+100$) m, bridging the primary channel of the Yangtze. Overall, the entire bridge stretches 1450 m. Geological assessments at the construction site revealed an absence of bedrock within a depth of 180 m, with fine sand predominating in the exposed layers. As a result, both the main and approach bridge foundations were constructed using large-diameter bored piles. To enhance the strength of the pile foundations and optimize costs, a combined post-grouting technique was implemented in this construction.

2.2. Soil layers and test piles

The project was located in the plain between the two lakes, where the exposed strata consist of loose sediments from the Quaternary System. No bedrock was found in drilling up to 180 m, with the nearest bedrock located deeper than 250 m near the bridge site. Based on geological age, genesis, lithological characteristics, and physical and mechanical properties, the strata were categorized into 8 major layers designated as Layers 1–8. To accommodate the substantial load of the superstructure, large-diameter pile foundations were utilized. Layer 7 comprised dense fine sand, exhibiting considerable thickness and stable distribution. In the upper section of the south bank, it is often interspersed with layers of pebble gravel. This layer presented favourable engineering geological conditions. Layer 8 predominantly consisted of Layer 8–3 of dense fine sand, intermixed with layers of pebble gravel and clay, exhibiting favourable engineering geological characteristics. Therefore, Layer 7 or Layer 8–3 was selected as the bearing layer. It is noteworthy that certain soil layers exhibited engineering properties similar to the fine sand layer, collectively referred to as the fine sand layers in this study. Table 1 summarizes the properties of soil layers at the site.

To obtain data for foundation design, pile load tests were conducted to assess bearing capacity at the main and approach bridges. Five test piles were selected for the main bridge, designated MB1 to MB5, while four test piles were chosen for the approach bridge, labelled AB1 to AB4. The elastic modulus of the concrete for the main bridge's five test piles and the approach bridge's four test piles was 31.5 GPa and 30.0 GPa, respectively. Except for AB1, which underwent pile side grouting for comparison, all other test piles from both the main and approach bridges employed the combined post-grouting method. The bearing layers at the pile tips for both bridges consisted of fine sand layers. The test piles for the main bridge were significantly longer compared to those of the approach bridge, resulting in an elevated grouting volume. Consequently, this study investigated the effect of the combined post-grouting technique on the pile load-bearing performance and the effect of combined grouting under conditions of varying pile length and cement quantity. Table 2 summarizes test pile specifications for both bridges.

3. The combined tip-and-side post-grouting technique

For both the main and approach bridges, the test piles employed a combined grouting approach, targeting both the pile tip and sides. Subsequently, a comprehensive evaluation was conducted to examine the pile load-bearing performance pre- and post-grouting, along with the surrounding soil conditions. This analysis was aimed at providing a detailed understanding of the efficacy of the combined post-grouting method.

The combined post-grouting system comprised two main components: the above-ground grouting system and the below-ground grouting system. Fig. 2 depicts the assembled grouting system. The above-ground grouting system included a grouting pump, mixer, grout storage tank, grouting piping system, pressure gauge, and pressure relief valve. The below-ground grouting system included grouting pipes at the pile tip and side within the reinforcement cage, along with grouting plugs. The grouting pipes were placed to ensure even distribution, ease of installation, and

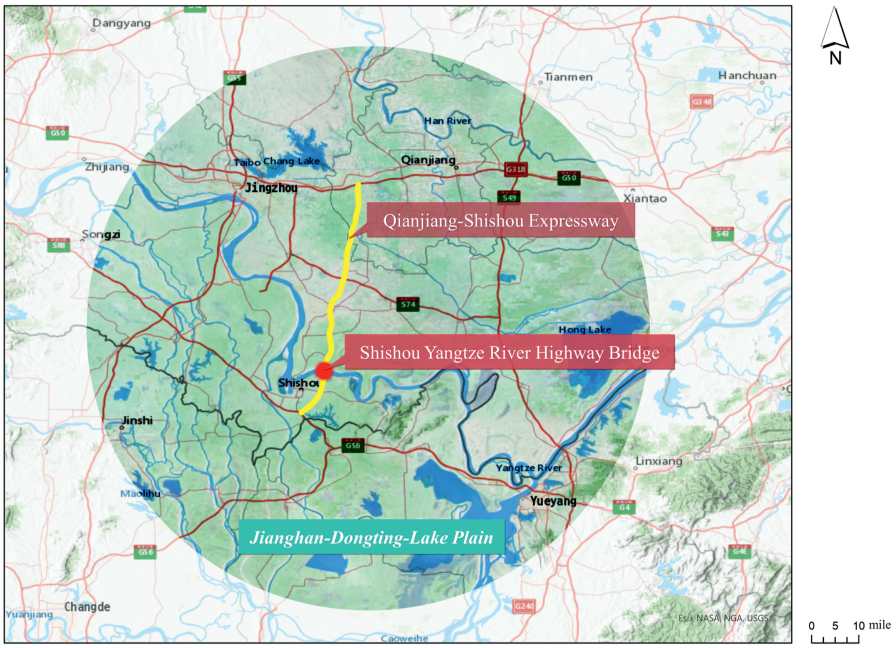

Fig. 1. Geographic location of the project.

Table 1
Soil parameters of the test site.

Layer No.	Soil name	γ (kN m^{-3})	c (kPa)	φ (°)	N_{SPT}	f_{sa} (kPa)	q_{sik} (kPa)
1–1	Clay	19.1	47	9.2	2–5	140	40
1–2	Silty clay	18.7	19	4.5	1–3	100	35
1–3	Silty soil	17.3	6	5.1	1–2	80	20
2	Clay	18.5	14	20.9	1–3	125	35
3	Fine sand	17.1	8	31.0	5–11	100	30
3–1	Silty clay	18.5	16	13.9	5–11	110	45
3–2	Sand	18.2	24	21.4	8–11	125	45
4	Fine sand	19.0	16	30.7	11–15	135	45
5	Fine sand	19.0	16	31.8	16–29	175	50
5–1	Clay	19.0	22	10.6	13–25	170	50
6	Fine sand	19.4	15	33.0	31–44	230	60
6–1	Silty clay	19.1	23	11.0	13–25	175	55
7	Fine sand	19.4	15	33.9	40–60	240	65
7–1	Silty clay	19.5	52	16.2	13–25	200	50
7–2	Boulder				60–70	450	130
7–3	Pebble				60–70	500	150
8–1	Pebble				70–180	550	155
8–2	Clay	19.9	54	16.6		250	70
8–3	Fine sand					250	65
8-3-1	Gravelly clay					260	70
8-3-2	Pebble					550	155

Note: γ, the unit weight; c, the cohesion of each soil layer; φ, the internal friction angle of each soil layer; N_{SPT}, the SPT index of each soil layer; f_{sa}, the basic allowable value of bearing capacity; and q_{sik}, the standard value of side resistance.

Table 2
Parameters of test piles.

Test site	Pile No.	D (m)	L (m)	L/D	Pile top elevation (m)	Bearing layer	Grouting method	Test phase
Main bridge	MB1	2.0	115	57.5	31.20	8-3 (Fine sand)	Combined	Before and after
	MB2	2.2	95	43.2	30.76	7 (Fine sand)	Combined	After
	MB3	2.2	115	52.3	29.60	8-3 (Fine sand)	Combined	Before and after
	MB4	2.2	120	54.5	29.60	8-3 (Fine sand)	Combined	Before and after
	MB5	2.0	110	55.0	31.20	8-3 (Fine sand)	Combined	Before and after
Approach bridge	AB1	2.0	50	25.0	33.80	7 (Fine sand)	Pile side	Before and after
	AB2	2.0	50	25.0	33.80	7 (Fine sand)	Combined	Before and after
	AB3	2.0	52	26.0	32.80	7 (Fine sand)	Combined	Before and after
	AB4	2.0	52	26.0	32.80	7 (Fine sand)	Combined	Before and after

Note: D, pile diameter; L, pile length; L/D, pile length-to-diameter ratio; Combined, the combined tip-and-side post-grouting; Pile side, the pile side post-grouting; Before and after, before and after post-grouting; and After, after post-grouting.

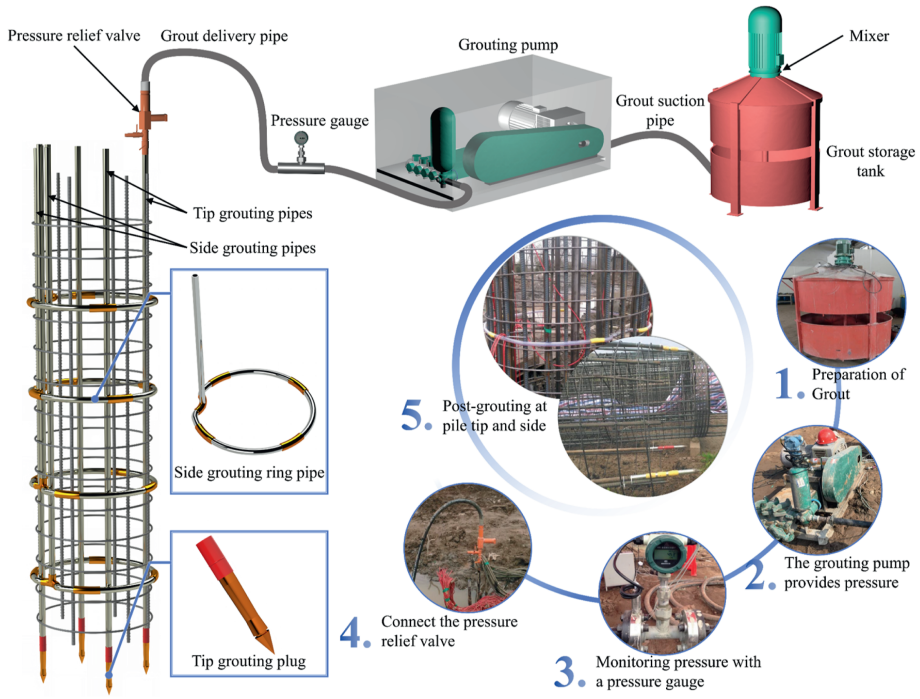

Fig. 2. Schematic diagram of the combined post-grouting technique.

protection. For this study, the grouting mechanisms for both the pile side and tip utilized the ring pipe and straight pipe methods, respectively.

Fig. 2 illustrates the configuration of the grouting pipeline along with the integrated post-grouting technique. This combined approach is notably more complex than performing grouting separately at the pile tip or side, as it incorporates procedures for both components. The construction process of combined post-grouting was categorized into three systems: the pile-soil system, the pumping system, and the grouting system. The pile-soil system involved the strategic arrangement of grouting pipes: the side ring pipe encircled the reinforcement cage externally, while the straight pipe at the pile tip was anchored within the cage and extended beyond its base. This configuration was crucial in laying the groundwork for effective grouting operations. The pumping system involved connecting the grouting equipment to the open plug after the pile concrete reached a certain strength, followed by water injection tests to determine key grouting parameters. The grouting system involved pushing the prepared grout into the soil layer at the pile tip and side using a grouting pump, enabling the grout to coalesce and solidify with the soil, with cement and water typically serving as the primary components for the grout material. To prevent potential damage to the pile concrete and address issues such as mud cake formation along the pile side and sediment residue at the pile tip, combined post-grouting was performed 28 d after concrete placement.

Grouting commenced with the pile sides, followed by the pile tip. For multiple side sections, grouting proceeded from top to bottom. The grout was channeled through the grouting pipe to the designated side ring pipe, where it was then dispersed into the surrounding soil via the grout ports located on the ring pipe. The tip grouting was directly transported from the grouting pipe to the tip grouting device for injection into the soil. Essential grouting parameters were dynamically monitored during construction via an automated control system and data acquisition framework. Grouting termination employed a dual-control approach based on grout volume and pressure, with the grouting volume serving as the primary control parameter. Fig. 3 illustrates the temporal variations in these critical grouting parameters (using test pile AB4 as an example), and Table 3 summarizes the grouting parameters for each test pile. Fig. 3 shows that both grouting flow rate and grouting pressure exhibit dynamic fluctuations over time. Moreover, the water-cement ratio also fluctuated during grouting. Initially, a ratio of 0.7 was used to ensure grout flow integrity. As grouting progressed, the ratio gradually decreased to a minimum of 0.5. The total cement quantity injected was 7.0×10^3 kg, with termination pressures for side and tip grouting ranging from 2.2 MPa to 4.2 MPa. The flow rate fluctuated within a band of 35–50 L per minute, and all grouting parameters met the practical requirements of the construction process.

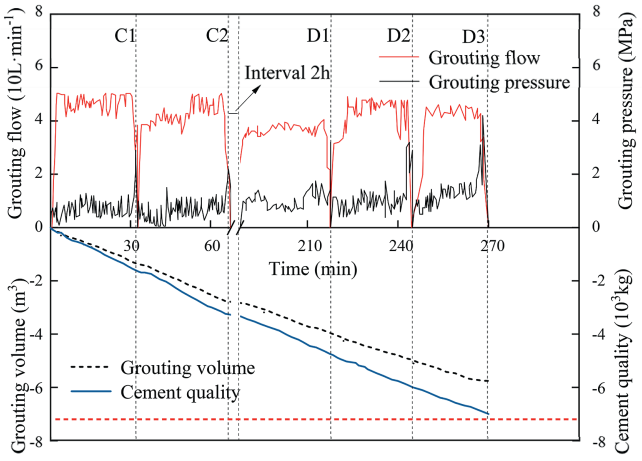

Fig. 3. Variation curves of essential parameters of grouting with time for test pile AB4 of the approach bridge.

Table 3
Grouting parameters.

Pile No.	Water-cement ratio	Quantity of cement (10^3 kg)		Grouting pressure (MPa)		Position of side pipes above the pile tip (m)
		Pile side	Pile tip	Pile side	Pile tip	C1, C2, C3, C4
MB1	0.65	6.0	3.9	4.2	10.0	20, 40, 60, 80
MB2	0.65	6.0	3.9	4.2	5.2	15, 30, 45, 60
MB3	0.65	7.3	4.0	4.0	4.3	20, 40, 60, 80
MB4	0.65	8.0	4.0	4.2	4.6	20, 40, 60, 80
MB5	0.65	6.0	3.8	4.4	9.6	20, 40, 60, 80
AB1	0.50	3.6	/	3.9	/	8, 23, 38, /
AB2	0.50	3.0	4.0	2.7	4.2	15, 30, /, /
AB3	0.50	3.4	3.6	2.8	4.3	15, 30, /, /
AB4	0.50	3.4	3.6	2.9	4.2	15, 30, /, /

Note: Only the grouting pressure of the first cross-section of the grouting pipe at the pile side is given. C1, C2, C3, and C4 indicate the distance of the first, second, third, and fourth annuli from the pile tip, respectively.

4. Test methods and data analysis

4.1. Static load test

The static load test is the most reliable method for evaluating pile foundation performance under service conditions, providing an accurate reflection of load-bearing behaviour. Consequently, it can be used to quantitatively evaluate the effectiveness of combined post-grouting (Cui et al., 2021). The static load test employed the slow maintained load method in two phases: (1) testing the trial pile before grouting, after the pile concrete reached the required strength; and (2) testing the same pile after grouting, once the cement grout had fully cured and attained the specified strength.

Using test piles MB3 and MB4 of the main bridge, and test piles AB1 and AB2 of the approach bridge as examples, this study analysed changes in the pile bearing performance before and after grouting. Fig. 4 illustrates the pile head load (Q) versus displacement (s) curves for each test pile.

In Fig. 4, AB1 underwent only pile side grouting, while the others underwent combined grouting. It can be observed that the Q-s curves of the test piles exhibit more pronounced inflection points before grouting. However, after grouting, the inflection points are displaced towards the position corresponding to the higher loads. Furthermore, the ultimate load-bearing capacity increases significantly. Initially, pile head displacement shows a linear relationship with load. However, as the load increases, the difference in performance before and after the grouting process becomes quite apparent. Prakash and Sharma (1990) and Zhang et al. (2014) recommend defining the ultimate load as the load preceding failure for a single pile. Thus, the ultimate bearing capacities of test piles MB3, MB4, AB1, and AB2 were found to be 46 MN, 57 MN, 21 MN, and 21 MN, respectively, before grouting. After the grouting, these values increased to 116 MN, 118 MN, 30 MN, and 37 MN. After grouting, the test piles met the design bearing capacity requirements, demonstrating a clear advantage over their pre-grouting state. At ultimate load, the bearing capacity of test piles MB3, MB4, AB1, and AB2 increased by 152 %, 107 %, 43 %, and 76 %, respectively. These results demonstrate that grouting markedly increases the ultimate bearing capacity of the piles and effectively limits pile head displacement under comparable loads. As illustrated in Fig. 4b, the ultimate bearing capacity of test pile AB2 increased notably after grouting, reaching approximately 177 % of the ultimate capacity of AB1. This significant difference demonstrates that combined post-grouting substantially outperforms side grouting alone in enhancing the load-bearing capacity of pile foundations.

Pile length is a key factor influencing pile bearing capacity. Consequently, the design of grouting volume must incorporate the consideration of pile length, as volume significantly impacts post-grouting efficacy. The diameters of the main bridge test piles, MB3 and MB4, are marginally greater than those of the approach bridge test piles, AB1 and AB2. Notably, the pile lengths of MB3 and MB4 are approximately double those of the approach bridge test piles.

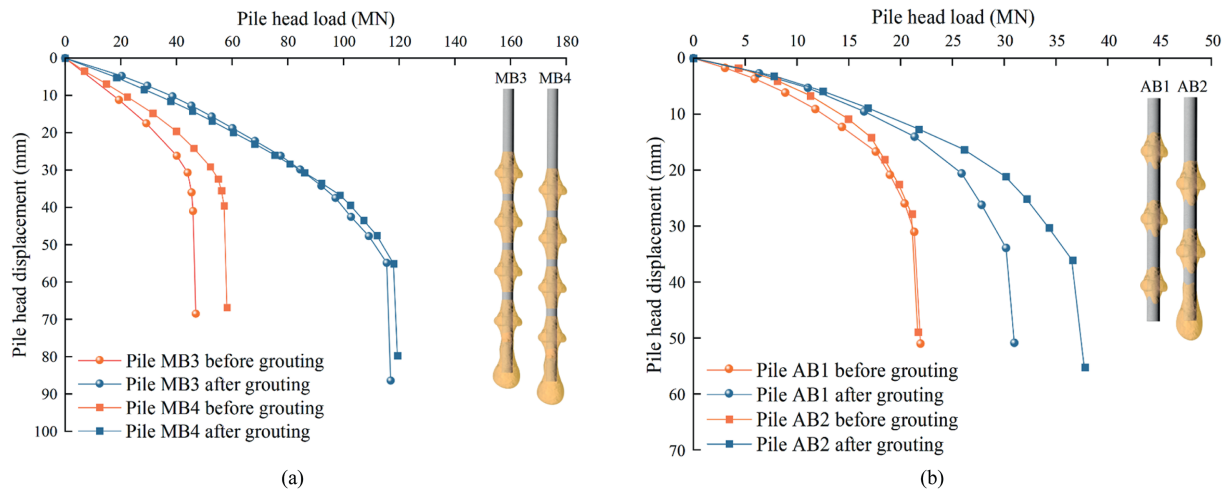

Fig. 4. Q-s curves of test piles for main and approach bridges. (a) MB3-MB4; and (b) AB1-AB2.

Analysis of Fig. 4 reveals that the bearing capacity of MB3 and MB4, which possess longer pile lengths, exhibits superior performance both before and after grouting compared to AB1 and AB2, while the bearing layers of these piles are both fine sand. Furthermore, Fig. 4 indicates that the improvement in ultimate bearing capacity for MB3 and MB4 following grouting is markedly higher than that observed for AB2, measuring 206 % and 145 % of the increase achieved by AB2, respectively. That is attributed to the greater pile side cement quantity applied to the longer main bridge test piles. Specifically, the total pile side cement quantity for MB3 was 143 % higher than for AB2, and for MB4 it was 167 % higher than for AB2.

Post-grouting pile side resistance is influenced by various factors such as pile parameters, soil layer properties, and grouting method. Side resistance at various depth ranges was calculated using static load test data and vibrating wire rebar strain gauges (a_1-a_n) positioned within the pile. Fig. 5 shows the distribution of side resistance versus depth at ultimate load for main bridge piles MB3 and MB4, and approach bridge piles AB1 and AB2.

Fig. 5a demonstrates a marked enhancement in the side resistance of test piles MB3 and MB4 at various depths following combined grouting. This indicates that combined grouting substantially increases the side resistance mobilized by the pile. Due to similar soil conditions and length-to-diameter ratios, the side resistance distributions along the depth for MB3 and MB4 are nearly identical, both before and after grouting. From Fig. 5b, it is evident that both pile side post-grouting and combined post-grouting effectively improve the side resistance characteristics of test piles AB1 and AB2 of the approach bridge. Grouting significantly enhanced side resistance. Although AB1 and AB2 had similar soil layers and length-to-diameter ratios, and the pre-grouting side resistance distributions were similar, the side resistance near the pile tip of AB2 after grouting was higher than that of AB1, primarily due to the difference in the pile side post-grouting and the combined post-grouting. Unlike the pile side post-grouting implemented in AB1, the combined post-grouting applied in AB2 caused grout to migrate upward from the pile tip, strengthening the soil within a specific range above the pile tip and increasing side resistance at that depth. Therefore, compared to pile side grouting alone, combined grouting offered advantages in enhancing the pile side resistance.

The total side resistance of test piles MB3 and MB4 for the main bridge, as well as AB1 and AB2 for the approach bridge, under ultimate load conditions before grouting, were 46 MN, 50 MN, 14 MN, and 14 MN, respectively. After grouting, the total side resistance increased to 103 MN, 102 MN, 23 MN, and 25 MN, respectively. Consequently, under ultimate load conditions after grouting, the total side resistance of test piles MB3, MB4, AB1, and AB2 increased by 124 %, 104 %, 64 %, and 79 %, respectively. The enhancement in total side resistance was considerably more pronounced for the longer main bridge test piles compared to the shorter approach bridge piles. This difference can be attributed to the greater total grouting volume applied along the sides of the main bridge test piles. Furthermore, both the total side resistance and its increase for AB2, which underwent combined grouting, were notably higher than for AB1, which underwent pile side grouting alone. This confirms the impact of upward grout migration from the tip on enhancing side resistance in combined grouted piles, as discussed. It demonstrates that combined grouting is more effective than pile side grouting alone.

4.2. Core drilling test

To visually evaluate the impact of the combined post-grouting within the deep fine sand layer, core drilling was performed approximately 50 d after grouting completion. The methods for pile tip and side core drilling, along with core hole arrangement, are illustrated in Fig. 6. Two symmetrically positioned core holes were placed on the outer side of the pile, 20 cm away from the steel casing, to assess the post-grouting effect along the pile side. The post-grouting effect at the pile tip was evaluated by using a ϕ130 mm steel tube secured to the inner side of the reinforcement cage in advance, and a 110 mm diameter drilling rig was used to extract core samples from the pile tip. As the pre-buried coring tubes were lowered into the hole alongside the cage, rubber bands were used to seal the bottom of each tube. This precaution was taken to ensure that no sediment or grout could infiltrate the pile tip during the process. The tops of the tubes were positioned 30 cm above the natural ground level. GXY-1 type drilling rigs were used to obtain samples from 8 pile side core holes from 4 test piles (MB1, MB2, MB4, and MB5) selected at the main bridge test site. Additionally, pile tip core sampling was performed on 5 test piles of the main bridge. At the approach bridge test site, core samples were taken from two pile side core holes of the side grouted pile AB1, while combined post-grouted piles AB3 and AB4 underwent both pile side and pile tip sampling. SPT tests were simultaneously conducted at the pile side locations of both the main and approach bridge test piles.

Full-core coring was conducted on the two pile side coring

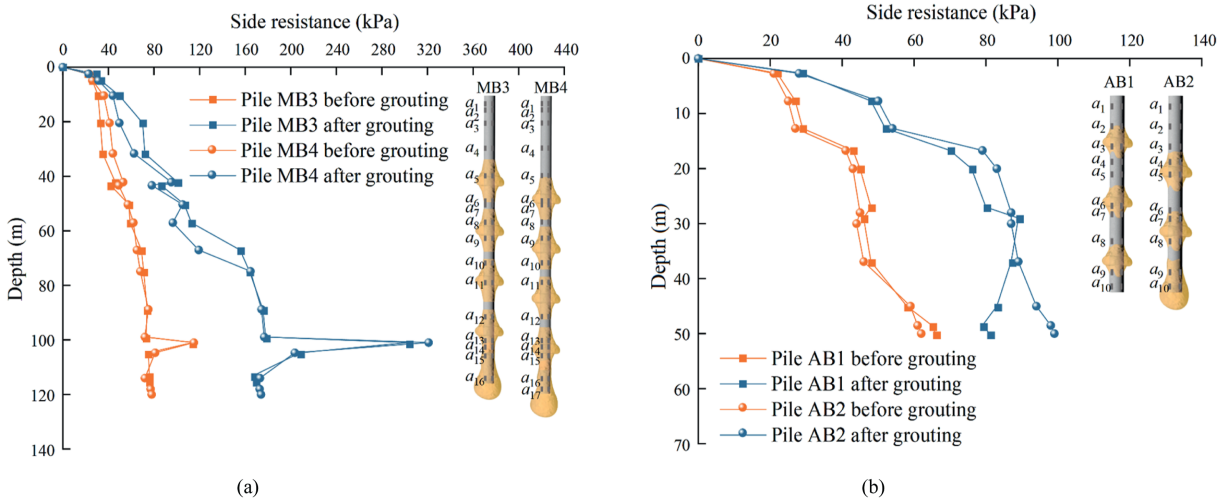

Fig. 5. The distribution curves of measured side resistance with depth under ultimate load for test piles of the main bridge and approach bridge. (a) MB3-MB4; and (b) AB1-AB2.

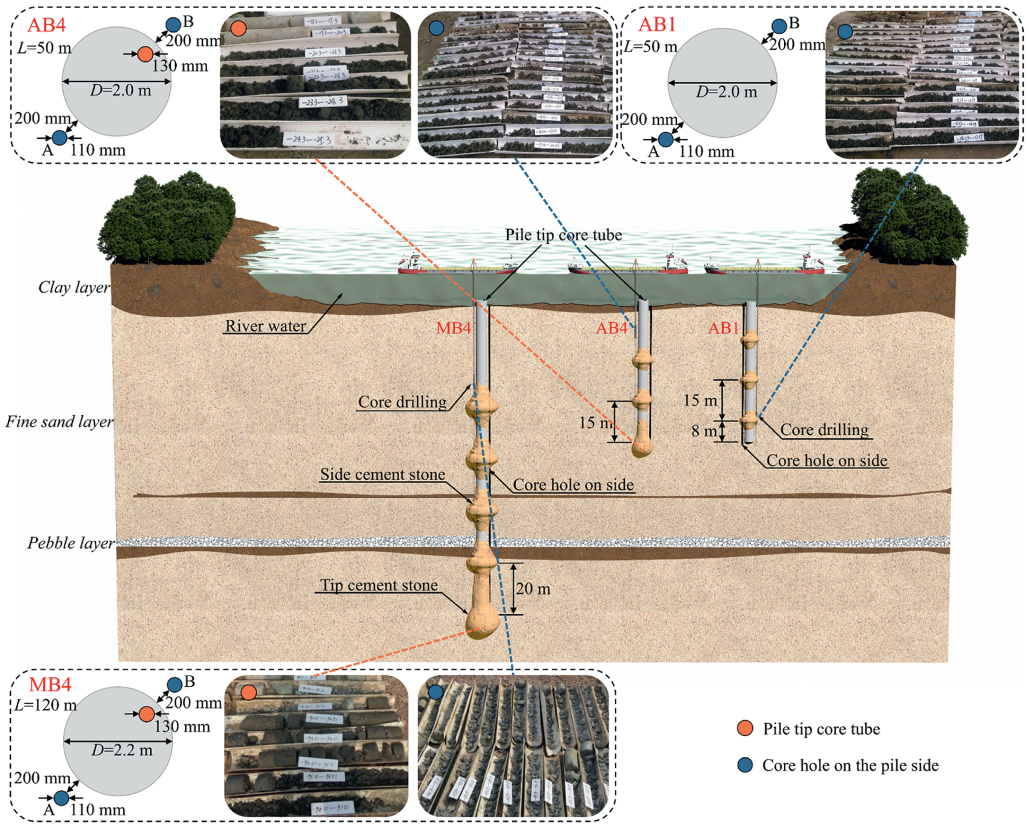

Fig. 6. Schematic diagram of the core drilling test of the main bridge and approach bridge test piles.

holes of the main bridge test piles MB1, MB2, MB4, and MB5, as well as the approach bridge test piles AB1, AB3, and AB4. Table 4 specifies the locations of the initial and final cement grout observed in each pile side coring hole for both the main and approach bridges. From Tables 4 and it can be observed that there is minimal difference in the depth of the initial and final cement grout in the two side coring holes of each test pile, and the final cement grout positions were all close to or below the pile tip, indicating that the pressurized grout upward migration and downward seepage strengthen the soil along the pile side. Grout upward migration for the closest ring pipe near the main bridge test pile tops ranges from 2 m to 8 m, compared to 5–12 m for the approach bridge. Fig. 6 presents schematic diagrams of the pile side core drilling for both the main and approach bridge test piles, along with some on-site photographs. As shown in Fig. 6, extracted core samples included loose lumps, columns, and short columns, with the penetration of grout into the fine sand soil layer being more pronounced. Core samples from the main bridge piles showed higher cement grout content due to the larger grout volume injected along the pile side. In contrast, core samples from the approach bridge piles exhibited discontinuous and uneven grout distribution, resulting in lower grout content. Core sample results from the MB4 pile side coring hole of the main bridge indicated the presence of cement grout within the depth range of 32.0–34.2 m, with the fourth layer of pressurized grout annulus (the nearest pressurized grout annulus from the pile top) located at a depth of 40 m. Around 60 m depth, the cement grout gradually thickened, with the third layer of pressurized grout annulus situated at a

Table 4
Results of pile side coring of test piles for main and approach bridges.

Pile No.	Core hole number	Pile top elevation (m)	Bottom hole elevation (m)	Pile length (m)	Depth of hole (m)	The depth of the initial cement grout (m)	The depth of the final cement grout (m)
MB1	Pile side A	31.2	−82.8	115.0	114.0	33.0	114.0
	Pile side B	31.2	−82.8	115.0	114.0	33.0	114.0
MB2	Pile side A	30.8	−67.5	95.0	98.3	35.6	98.3
	Pile side B	30.8	−67.5	95.0	98.3	33.6	98.3
MB4	Pile side A	29.6	−91.2	120.0	120.8	32.0	120.8
	Pile side B	29.6	−91.2	120.0	120.8	32.6	120.8
MB5	Pile side A	31.2	−80.7	110.0	111.9	36.2	111.9
	Pile side B	31.2	−80.7	110.0	111.9	35.1	109.9
AB1	Pile side A	33.8	−19.7	50.0	53.5	14.9	53.5
	Pile side B	33.8	−18.4	50.0	52.2	13.7	52.2
AB3	Pile side A	32.8	−21.7	52.0	54.5	13.2	54.5
	Pile side B	32.8	−22.3	52.0	55.1	13.4	55.1
AB4	Pile side A	32.8	−20.5	52.0	53.3	8.6	53.3
	Pile side B	32.8	−20.3	52.0	53.1	10.1	53.1

depth of 60 m. At a position 10 m above the pile tip, the cement grout was thickest, appearing in the form of columns or short columns. Consequently, the findings from the core drilling analysis reinforce the notion that the slight variation in side resistance observed before and after the grouting process, within the depth span of 0–20.4 m during the static load test, can be ascribed to insufficient pressurized grout upward migration within this upper pile section.

Pile tip core drilling was conducted on the reserved coring tubes of test piles MB1-MB5 of the main bridge, as well as test piles AB3 and AB4 of the approach bridge. The range of pile tip core drilling and the initial and final positions of the cement grout can be found in Table 5. According to Table 5, the depth range affected by grouting at the pile tip for the main bridge test piles was approximately 3.1–6.0 m below the pile tip (about 1.4*D*–3.0*D*), while the maximum depth range of reinforcement after grouting at the pile tip for the approach bridge was about 4.5–5.3 m below the pile tip (about 2.3*D*–2.7*D*). Pile tip grouting can bolster both the strength and stiffness of the soil in the immediate vicinity of the pile tip. This, in turn, noticeably bumped up the tip bearing resistance, leading to a stronger pile foundation overall. This observation lines up perfectly with the findings from the static load test. Fig. 6 includes images of pile tip coring for the main and approach bridges. As observed from Fig. 6, grout density was higher in the pile core tips. The majority of core samples extracted from the main bridge test piles were predominantly columnar or short columnar configuration, whereas those gathered from the approach bridge test piles were typically loose aggregates. The cement grout located nearer to the tip of the pile contains a higher cement proportion, enhancing and fortifying the surrounding soil layer to a specific depth beneath the pile tip. It is important to highlight that, despite 50 d having elapsed since the grouting of the test piles, some cement grout at the pile tip remained unset.

4.3. Standard penetration test

The standard penetration test (SPT) is a widely used dynamic penetration method in geotechnical field assessments. This method boasts simple equipment, ease of use, and yields relatively straightforward results (Boulanger et al., 2012; Guan and Wang, 2022; Bol, 2023; Gao et al., 2023; Viviescas, 2023). Frequently conducted alongside core drilling, SPT is suitable for evaluating post-grouting efficacy.

During the post-grouting process, the mixing and solidification of cement grout with the soil layer at the pile tip and side result in the formation of cemented soil reinforcement, causing significant disparities in the properties and conditions between the original soil layer and the cemented soil reinforcement. Consequently, the blow counts required to reach an equivalent depth in the soil layer may differ. Therefore, the reinforcement effect can be assessed by observing the changes in the N_{SPT} values before and after grouting. In this experiment, the SPT was conducted on the main bridge test piles MB1, MB2, MB4, and MB5, as well as the approach bridge test piles AB1, AB3, and AB4, to evaluate the grouting effect by comparing the SPT indices before and after grouting. For the main bridge test piles, the SPT was initiated approximately 30 m below the natural ground level in the core holes along the pile side, with penetrations performed at 10-m intervals. For approach bridge test piles, the SPT was initiated around 7–10 m below the natural ground level of the pile side core holes, with penetrations executed every 5-m interval.

Comprehensive SPTs were performed adjacent to seven test piles for both the main and approach bridges, on 14 core samples from the sides of the piles. The SPT indices obtained from sides A and B of the piles post-grouting were analysed alongside the SPT data from the corresponding exploratory holes drilled before grouting. Fig. 7 compares the comparative distribution of the SPT indices for the test piles, highlighting the differences observed before and after the grouting process for both bridge sections.

As shown in Fig. 7, the SPT index trends with depth for the test piles of both the main and approach bridges were consistent between sides A and B post-grouting, with minor discrepancies between the core hole measurements. For the main bridge piles, the SPT index increase was more pronounced in the lower pile section than in the upper, particularly below 60 m depth, where significantly higher indices were recorded. Furthermore, the cement grout in the core samples obtained at depths of approximately 60 m during the core drilling test exhibited a progressively higher concentration. The relatively smaller increase in SPT index at a depth of around 30 m may be attributed to insufficient grout upward migration from the fourth pressurized annulus within this range. Notably, the SPT index derived from the pile side B core hole of test pile MB1 did not exhibit significant improvement compared to before grouting, indicating non-uniform filling and discontinuous distribution of the grout pressed along the pile side. Fig. 7 also shows that the approach bridge test piles displayed a greater increase in SPT index from the position of the second layer of pressurized grout ring pipe to the pile tip, indicating that upward grout migration and downward seepage within this interval compacted the surrounding soil adjacent to the pile. Overall, post-grouting SPT indices were higher than pre-grouting values, signifying that the cement grout filled defects on the pile-soil contact surface, enhanced the boundary conditions of the pile-soil interface after curing, and altered the physical and mechanical properties of the soil along the pile side. This increased side resistance and pile-soil interface roughness, improved pile side soil strength and stiffness, and consequently led to a significant increase in the SPT index of the surrounding soil after grouting compared to before grouting.

5. Method of predicting side resistance based on SPT index

The SPT index and pile side resistance exhibited similar distribution patterns with depth. Therefore, a statistical approach

Table 5
Results of pile tip coring of test piles for main and approach bridges.

Pile No.	Pile top elevation (m)	Bottom hole elevation (m)	Pile length (m)	Depth of hole (m)	The depth of the initial cement grout (m)	The depth of the final cement grout (m)	Depth of pile tip grouting (m)
MB1	31.2	−91.9	115.0	123.1	115.1	121.1	6.0
MB2	30.8	−69.1	95.0	99.9	96.0	99.6	3.6
MB3	29.6	−84.5	115.0	114.1	116.8	119.9	3.1
MB4	29.6	−97.5	120.0	127.1	121.9	126.8	4.9
MB5	31.2	−86.7	110.0	117.9	111.9	117.5	5.6
AB3	32.8	−25.3	52.0	58.1	52.5	57.8	5.3
AB4	32.8	−24.6	52.0	57.4	52.6	57.1	4.5

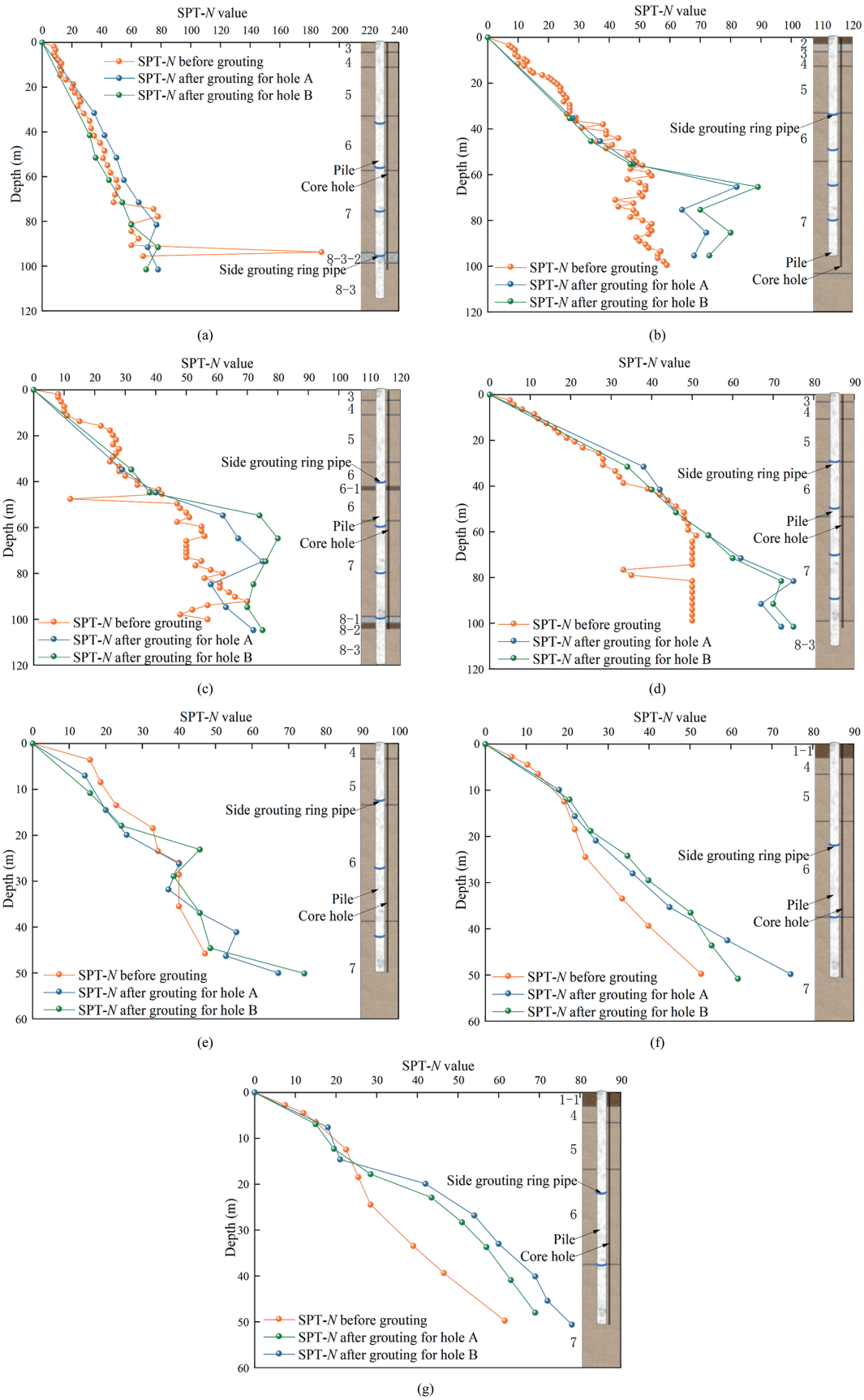

Fig. 7. Comparison of the number of standard penetration blows before and after grouting of test piles for the main and approach bridges. (a) MB1; (b) MB2; (c) MB4; (d) MB5; (e) AB1; (f) AB3; and (g) AB4.

was employed to calculate the side resistance at each depth with the SPT index, both before and after grouting. The calculation of side resistance for bored piles predominantly utilizes the empirical formula $q_{su} = K_s N_{SPT}$, where K_s represents the empirical coefficient specifically associated with side resistance and the N_{SPT} index. Shioi and Fukui (1982) suggested $K_s = 2$, GEO (2006) proposed $K_s = 1.4$, and Xiao and Yang (2011) recommended $K_s = 3$ for the Singapore region. Various K_s values were provided in the literature, such as Meyerhof (1956), Aoki and Velloso (1975), Meyerhof (1976), and Chang and Broms (1991). Thus, the empirical coefficient of side resistance, K_s, is somewhat geographically and contextually limited.

To determine the empirical coefficient K_s for side resistance in Shishou's fine sand layer, statistical analysis was performed on the SPT indices obtained from 14 side core holes of 7 test piles, MB1, MB2, MB4, and MB5 of the main bridge, and AB1, AB3, and AB4 of the approach bridge. Fig. 8 illustrates the relationship between pre- and post-grouting SPT indices within the fine sand layer. Fig. 9 depicts the relationship between side resistance and SPT indices, both before and after grouting.

Fig. 8 illustrates the relationship between the SPT indices before and after grouting, which were fitted using a nonlinear power function ($N'_{SPT} = aN^b_{SPT}$). The fitted relationship can be expressed as

$$N'_{SPT} = 1.32N^{0.98}_{SPT} \tag{1}$$

where N'_{SPT} is the number of the SPT index after grouting, and N_{SPT} is the SPT index before grouting. The fitted parameters are $a = 1.32$ and $b = 0.98$.

As illustrated in Fig. 9, the side resistance in the fine sand layer shows a noticeable upward trend alongside rising SPT indices, both before and after the grouting. In Fig. 9a, the solid line depicts a linear correlation between the side resistance and the SPT index before grouting, which can be roughly expressed by

$$q_{su} = 1.44N_{SPT} \tag{2}$$

where q_{su} is the pre-grouting side resistance, and N_{SPT} is the pre-grouting SPT index. The empirical coefficient of side resistance before grouting is $K_s = 1.44$.

Similarly, the solid line in Fig. 9b represents a linear relationship between the side resistance and the SPT index after grouting, fitted with the following approximation equation:

$$q'_{su} = 2.28N'_{SPT} \tag{3}$$

where q'_{su} is the post-grouting side resistance, and N'_{SPT} is the post-grouting SPT index. The empirical coefficient of side resistance after grouting is $K_s = 2.28$.

By substituting Eq. (1) into Eq. (3), the correlation between post-grouting side resistance and pre-grouting SPT index is defined as

$$q'_{su} = 3.01N^{0.98}_{SPT} \tag{4}$$

where q'_{su} is the post-grouting side resistance, and N_{SPT} is the pre-grouting SPT index.

To validate the accuracy and applicability of the derived empirical coefficients presented in this paper, the main bridge test pile MB3 and the approach bridge test pile AB2 of the Shishou Yangtze River Highway Bridge were selected as calculation examples. Using the pre-grouting SPT indices in the corresponding exploration holes of the two test piles, the side resistance before and after grouting was calculated using Eqs. (2) and (4), respectively. The results for the side resistance of test piles MB3 and AB2, both before and after grouting, were obtained and juxtaposed with the measured side resistance values, as illustrated in Fig. 10.

As shown in Fig. 10, the calculated values of side resistance before and after grouting of the two test piles show good agreement with the measured values, indicating that the derived empirical coefficients K_s for the fine sand layer before and after grouting are applicable. Therefore, these empirical coefficients can be used as an engineering design for the fine sand layer in the Shishou area. Moreover, in accordance with Eqs. (2) and (4), the side resistance of the fine sand layer before and after grouting can be estimated based solely on the pre-grouting SPT index. This simplifies the estimation process and provides a more scientific and reliable approach. Consequently, using the pre-grouting SPT index to estimate side resistance is straightforward and facilitates more scientifically rigorous and reliable pile foundation design.

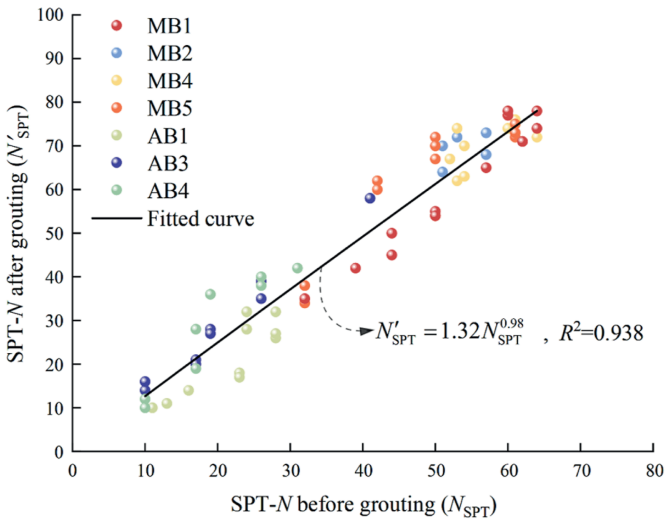

Fig. 8. The relationship between the SPT index before and after grouting.

6. Discussion

This study provided a comprehensive and detailed assessment of the combined post-grouting effect using various testing methods. Among these, the static load test proved to be the most straightforward and efficient, although it was site-specific and costly. Core drilling and SPT offered advantages in equipment simplicity and ease of use, making them suitable for practical engineering applications. However, as both core drilling and SPT were point-specific vertical tests, they only recorded the distribution of grout and blow count in one-dimensional direction and could not fully characterize the reinforcement of soil by combined post-grouting. They had spatial limitations and caused some soil disturbance around the pile. Consequently, multidimensional non-destructive testing techniques warrant further investigation for assessing the efficacy of integrated post-grouting moving forward. Iliopoulos et al. (2016) proposed the integration of X-ray and ultrasonic pulse velocity (UPV) methods for non-destructive evaluations of grouted joints in offshore wind turbine monopiles. Huang et al. (2022) applied elastic wave computerized tomography (CT) to assess the effectiveness of grouting in bridge pile foundations, visualizing the spatial distribution of grout in the reinforced area. Hu et al. (2022) utilized a testing method combining transmitted wave and power touch probing to evaluate the effects on soil layers after pile foundation grouting. The methods reported above can all be used to evaluate the effectiveness of pile foundation grouting.

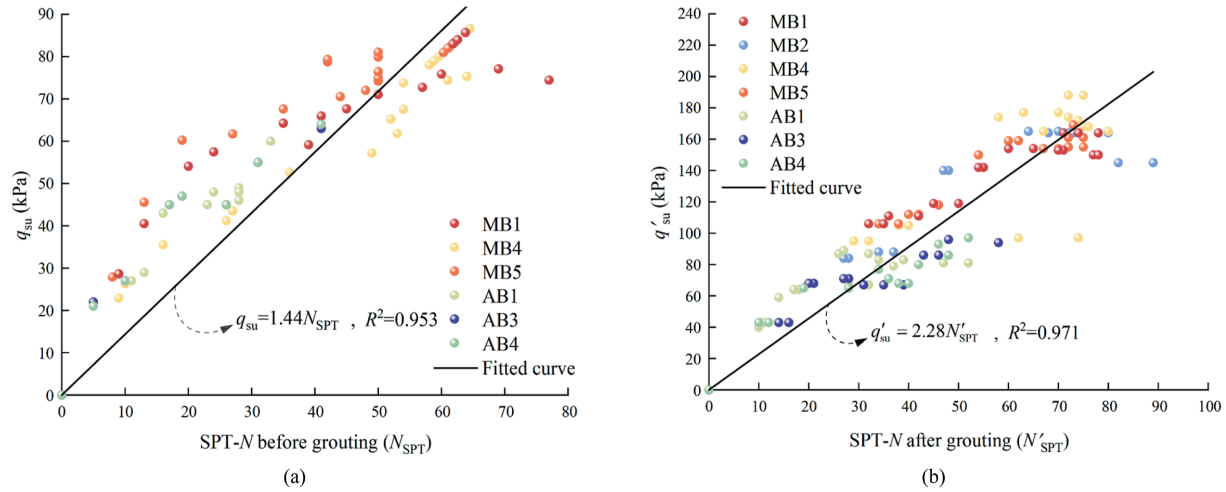

Fig. 9. The relationship between the side resistance and the SPT index before and after grouting: (a) Before grouting, and (b) after grouting.

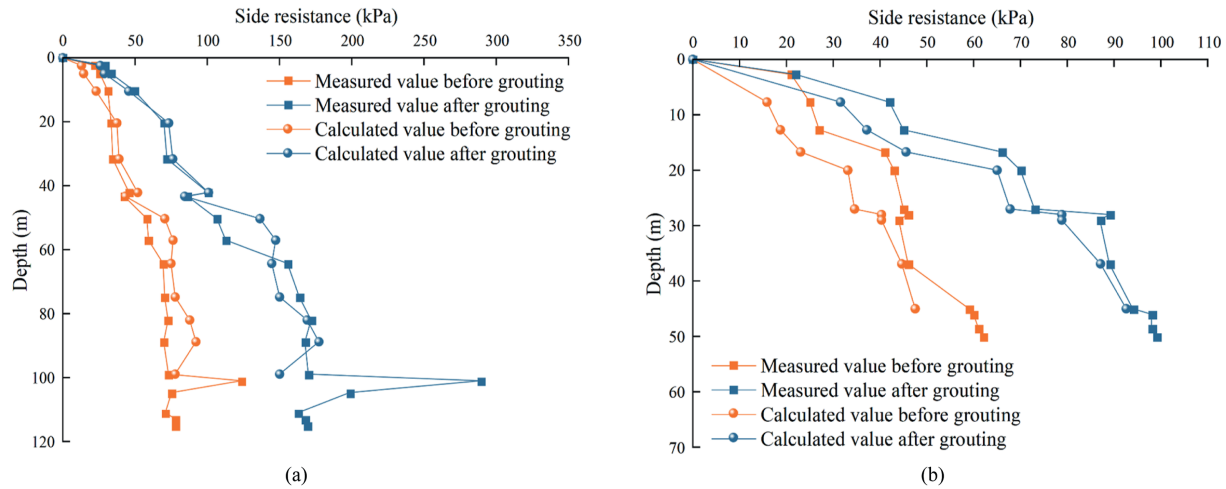

Fig. 10. Comparison of measured and calculated pile-side resistance before and after grouting: (a) MB3; and (b) AB2.

Future comprehensive evaluation of the combined post-grouting effect could integrate CT scanning, ultrasonic waves, geo-radar, and traditional exploration methods. Current methods primarily evaluate the final effect and lack real-time monitoring capabilities during the grouting process. Therefore, dynamic monitoring methods during the combined grouting process are also necessary research subjects for the future.

Many scholars have proposed empirical coefficients for calculating side resistance based on the SPT index. However, these coefficients vary considerably and are region-specific, leading to significant variations in calculating the pile bearing capacity across different regions, soil layers, and operational conditions. In recent years, Artificial Intelligence (AI) has demonstrated notable capabilities in predicting the pile foundations' bearing capacity. Fatehnia and Amirinia (2018) reviewed the application of Genetic Programming (GP) and Artificial Neural Network (ANN) in estimating pile-bearing capacity. They conducted statistical analyses on the frequency of use of input variables such as pile length, SPT, Cone Penetration Test (CPT), and soil conditions to gain a clearer insight into the significance of various variables and inspire the inclusion of other relevant input variables. Zhang and Goh (2016) and Zhang et al. (2019) conducted in-depth studies on pile drivability by applying machine learning algorithms such as Multivariate Adaptive Regression Splines (MARS) and Random Forest Regression (RFR). They developed effective models to predict the maximum compressive stress and blows per foot (BPF) of piles, emphasizing the importance of feature selection and regularization in enhancing model performance. Pierre et al. (2021) further demonstrated the reliable prediction of jet grouting pile diameters through optimizing ANNs using the Differential Evolution (DE) algorithm. Numerous studies have highlighted the significant potential of machine learning algorithms, including Random Forest, Deep Neural Networks, and XGBoost, in the field of pile foundation engineering (Nguyen et al., 2022; Pham and Tran, 2022; Esteban et al., 2024; Tan et al., 2024; Tram et al., 2024). Based on these findings, applying these methods to post-grouted piles is highly feasible. By leveraging machine learning, it's possible to assess how different factors impact the load-bearing capacity of piles and even forecast the outcomes of grouting in post-grouted piles. The application of AI in post-grouted pile foundation engineering represents a meaningful and promising research direction.

7. Conclusions

This study relied on nine bored piles of the Shishou Yangtze River Highway Bridge project to comprehensively evaluate the effectiveness of combined tip-and-side grouting through static load tests, core drilling, and SPT, and compare it with side grouting. Moreover, it also investigated the impact of pile length on the bearing capacity of pile foundations and the role of cement quantity on combined grouting efficacy. Finally, through statistical methods, it established a combined grouting method based on the SPT index before and after grouting, as well as a functional relationship formula to predict the post-grouting side resistance based on the SPT index before grouting. The following conclusions can be derived from the test outcomes and analyses.

(1) Static load tests demonstrated a significant increase in pile-bearing capacity post-combined grouting, showing ultimate capacity gains between 76 % and 152 %. Combined post-grouting demonstrated enhanced performance compared to side-grouting alone. The ultimate bearing capacity of combined post-grouted piles was approximately 177 % of side-grouted piles. This enhancement was attributed to improved initial soil stiffness at both the pile tip and side, increasing both tip and side resistance.
(2) The outcomes of static load tests carried out on test piles of different lengths revealed that longer piles tend to have an increased contact area with the surrounding soil, resulting in noticeably better bearing capacity when compared to their shorter counterparts. Furthermore, the side grouting volume was higher for longer piles, which makes the combined grouting effect more significant. Specifically, when comparing piles with lengths differing by a factor of two, the longer piles exhibited an ultimate bearing capacity exceeding 215 % of that of the shorter piles. Under conditions where the total side cement quantity was increased to approximately 250 % of the original, the bearing capacity of longer piles could be up to 206 % of that of shorter piles.
(3) The results of core drilling at the pile tip and side showed a significant grouting effect, with cement grout upward migrated to over 2 m for the main bridge test piles, and the reinforcement depth at the pile tip was approximately 1.4D to 3.0D below the pile tip. For the approach bridge test piles, cement grout upward migrated to 5 m above the ground, with the reinforcement depth at the pile tip ranging from approximately 2.3D to 2.7D below the pile tip. Following the application of combined post-grouting techniques, cement grout permeated, upward migrated, and spread into the fine sand, reinforcing the soil layers beneath the pile tip and along its sides. This process optimized the stress distribution at the pile-soil interface, ultimately increasing the load-bearing capacity of the foundation.
(4) Standard penetration tests showed a notable boost in the SPT index for the soil surrounding the pile after combined post-grouting, and a similar distribution pattern of side resistance along the depth, indicating a significant increase in side resistance due to combined post-grouting. Statistical analysis showed side resistance coefficients for the fine sand layer as 1.44 pre-grouting and 2.28 post-grouting, facilitating side resistance estimation. Additionally, a functional relationship formula between side resistance and SPT index before grouting was established, facilitating estimation of side resistance after grouting and enabling more scientific pile foundation design. This calculation approach guided analogous projects involving fine sand layers.

CRediT authorship contribution statement

Zhihui Wan: Writing – review & editing, Writing – original draft, Supervision, Resources, Project administration, Methodology, Funding acquisition, Formal analysis, Data curation, Conceptualization. **Zilong Guo:** Writing – review & editing, Writing – original draft, Validation, Methodology, Data curation. **Guoliang Dai:** Writing – review & editing, Supervision, Resources, Project administration, Data curation. **Feng Zhou:** Writing – review & editing, Validation, Resources, Project administration, Data curation.

Declaration of competing interest

The authors declare that they have no known competing financial interests or personal relationships that could have appeared to influence the work reported in this paper.

Acknowledgments

This work was supported by the National Natural Science Foundation of China (Grant No. 52008100), China Postdoctoral Science Foundation (Grant No. 2022M723534), and the Natural Science Foundation of Jiangsu Higher Education Institutions of China (Grant No. 23KJA560005).

List of symbols

N_{SPT}	Standard penetration test index before grouting
γ	Unit weight of the soil
c	Cohesion of the soil
φ	Internal friction angle of the soil
f_{sa}	Basic allowable value of bearing capacity
q_{sik}	Standard value of pile side resistance
L	Pile length
D	Pile diameter
Q	Pile head load
s	Pile head displacement
K_s	Empirical coefficient associated with pile side resistance and the SPT index
N'_{SPT}	Standard penetration test index after grouting
q_{su}	Pile side resistance before grouting
q'_{su}	Pile side resistance after grouting

References

Aoki, N., Velloso, D.A., 1975. An approximate method to estimate the bearing capacity of piles. In: Proceedings of 5th Pan-American Conference of Soil Mechanics and Foundation Engineering, 1. International Society of Soil Mechanics and Geotechnical Engineering, Buenos Aires, pp. 367–376.
Bol, E., 2023. A new approach to the correlation of SPT-CPT depending on the soil behavior type index. Eng. Geol. 314, 106996.
Boulanger, R.W., Wilson, D.W., Idriss, I.M., 2012. Examination and reevalaution of SPT-Based liquefaction triggering case histories. J. Geotech. Geoenviron. Eng. 138 (8), 898–909.
Chang, M.F., Broms, B.B., 1991. Design of bored piles in residual soils based on field-performance data. Can. Geotech. J. 28 (2), 200–209.
Cui, Y., Qi, C., Zheng, J., Wang, X., Zhang, S., 2021. Field test research on post-grouting effect for super-long cast-in-place bored pile in thick soft foundation. Geotech. Geol. Eng. 39 (7), 4833–4842.
Esteban, D., Edgar, L.S.M., Roberto, T., 2024. Assessment of compressive strength of jet grouting by machine learning. J. Rock Mech. Geotech. Eng. 16 (1), 102–111.
Fatehnia, M., Amirinia, G., 2018. A review of Genetic Programming and artificial Neural network applications in pile foundations. Int. J. Geo-Eng. 9 (1), 2.
Gao, B., Zhang, Q., Zhu, W., Ye, G., Bao, X., 2023. Optimize characteristic value of SPT for seismic design of offshore wind turbines in liquefiable soils by stochastic models. Soil Dynam. Earthq. Eng. 172, 108045.
GEO, 2006. Foundation Design and Construction. Geotechnical Engineering Office, Hong Kong.
Gong, W., Zhang, Z., Lin, Y., Dai, G., Huang, H., 2023. Full-scale field test study of

bearing characteristics of post-grouting pile for offshore wind turbines. Ocean. Eng. 268, 113451.
Gouvenot, D., Gabaix, J.C., 1975. A new foundation technique using piles sealed by cement grout under high pressure. In: 7th Annual Offshore Technology Conference. OTC, Houston, pp. 645–656.
Guan, Z., Wang, Y., 2022. SPT-based probabilistic evaluation of soil liquefaction potential considering design life of civil infrastructures. Comput. Geotech. 148, 104807.
Ho, C.E., 2003. Base grouted bored pile on weak granite. In: Grouting Ground Treat, pp. 716–727.
Homma, Y., 2014. Introduction of base enlarged pre-boring method with nodular pile. In: The 1st Workshop on New Pile Foundation Technologies in Vietnam. Ho Chi Minh City. Ho Chi Minh University of Technology, Vietnam National University.
Horiguchi, T., Karkee, M.B., 1995. Load tests on bored PHC nodular piles in different ground conditions and the bearing capacity based on simple soil parameters. AIJ J. Technol. Des. 1 (1), 89–94.
Hu, H., Jin, Q., Yang, F., et al., 2022. A novel method for testing the effect of base post-grouting of super-long piles. Appl. Sci. 12 (21), 10996.
Huang, S., Cao, H., Liu, J., Yan, R., Zhang, H., 2022. Study on the application of elastic wave CT technique to detect the effect of post-grouting of pile foundation. Appl. Sci. 13 (1), 456.
Huynh, V.H., Nguyen, T., Nguyen, D.P., Nguyen, T.S., Huynh, T.M.D., Nguyen, T.C., 2022. A novel direct SPT method to accurately estimate ultimate axial bearing capacity of bored PHC nodular piles with 81 case studies in Vietnam. Soils Found. 62 (4), 101163.
Iliopoulos, A.N., Van, H.D., Vlassenbroeck, J., Aggelis, D.G., 2016. Assessment of grouted samples from monopile wind turbine foundations using combined non-destructive techniques. Constr. Build. Mater. 122, 855–862.
Lin, S.S., Lin, T., Chang, L.T., 2000. A case study for drilled shafts base mud treatment. In: New Technological and Design Developments in Deep Foundations. ASCE, Denver, pp. 46–58.
Littlechild, B.D., Plumbridge, G.D., Free, M.W., 1998. Shaft grouted piles in sand and clay in Bangkok. In: Proceedings of the 7th International Conference and Exhibition on Piling and Deep Foundations. ASCE, Reston, pp. 171–178.
Liu, S., Zhang, Q., Li, H., Yu, X., Liu, G., Cui, W., 2023. An analysis method for the response of combined side-and-tip grouting pile. Acta Geotech 18 (7), 3715–3729.
Ma, H., Ma, Y., Yao, W., Chen, C., 2021. Research on bearing capacity of post-grouting super-long bored pile. In: IOP Conference Series: Earth and Environmental Science, 634. IOP Publishing, 012111, 1.
Meyerhof, G.G., 1956. Penetration tests and bearing capacity of cohesionless soils. J. Soil Mech. Found Div. 82 (SM I), 1–19.
Meyerhof, G.G., 1976. Bearing capacity and settlement of pile foundations. J. Geotech. Eng. Div. 102 (GT3), 195–228.
Nguyen, M.H., Fellenius, B.H., 2015. Bidirectional cell tests on not-grouted and grouted large-diameter bored piles. J. GeoEngin. Sci. 2 (3), 105–117.
Nguyen, T., Ly, K.D., Nguyen-Thoi, T., Nguyen, B.P., Doan, N.P., 2022. Prediction of axial load bearing capacity of PHC nodular pile using Bayesian regularization Artificial Neural Network. Soils Found. 62 (5), 101203.
Pham, T.A., Tran, V.Q., 2022. Developing Random Forest hybridization models for estimating the axial bearing capacity of pile. PLoS One 17 (3), e0265747.
Pierre, G.A.N., Shen, S.L., Zhou, A., Giuseppe, M., 2021. Artificial neural network optimized by differential evolution for predicting diameters of jet grouted columns. J. Rock Mech. Geotech. Eng. 13 (6), 1500–1512.
Prakash, S., Sharma, H.D., 1990. Pile Foundations in Engineering Practice. John Wiley & Sons, New York, NY, USA.
Shioi, Y., Fukui, J., 1982. Application of N-value to design of foundations in Japan. In: Proceeding of the Second European Symposium on Penetration Testing, pp. 159–164. Amsterdam.
Tan, N., Ly, D.K., Jim, S., Phi, N.D., 2024. Optimizing load-displacement prediction for bored piles with the 3mSOS algorithm and neural networks. Ocean. Eng. 304, 117758.
Tram, B.N., Tan, N., Minh-The, N.Q., Jim, S., 2024. Predicting load–displacement of driven PHC pipe piles using stacking ensemble with Pareto optimization. Eng. Struct. 316, 118574.
Viviescas, J.C., 2023. Probabilistic analyses of a post-grouted anchor–soil bond friction performance considering the geological origin and the SPT-N tendency with depth. Int. J. GeoMech. 23 (1), 06022038.
Wan, Z.H., Duan, C., Hu, T., Zhou, F., Dai, G.L., 2024. Field study on bearing capacity of large-diameter rock-socketed bored piles with combined grouting in highly weathered rock layers. Rock Mech. Rock Eng. 57, 8701–8722.
Xiao, D.P., Yang, H., 2011. Back analysis of static pile load test for SPT-based pile design: a Singapore experience. In: Advances in Pile Foundation, Geosynthetics, Geoinvestigations, and Foundation Failure Analysis and Repairs. ASCE, pp. 144–152.
Zhang, Q.Q., Li, S.C., Li, L.P., 2014. Field study on the behavior of destructive and non-destructive piles under compression. Mar. Georesour. Geotechnol. 32 (1), 18–37.
Zhang, W.G., Goh, A.T.C., 2016. Multivariate adaptive regression splines and neural network models for prediction of pile drivability. Geosci. Front. 7, 45–52.
Zhang, W.G., Wu, C.Z., Li, Y.Q., Wang, L., Samui, P., 2019. Assessment of pile drivability using random forest regression and multivariate adaptive regression splines. Georisk 15 (1), 27–40.
Zhang, Z., Gong, W., Dai, G., Xu, J., 2021. Enhancement of load bearing of post-grouted drilled shafts based on in situ tests. Arabian J. Geosci. 14 (1), 32.

Dr. Zhihui Wan is an Associate Professor and Master's Supervisor at Nanjing Tech University, where he also serves as Deputy Director of the Institute of Underground Engineering Safety and Protection. He is recognized as a Jiangsu Provincial Association for Science and Technology Young Talent Lifting Project awardee and an Outstanding Young Scientific and Technological Talent in Engineering Construction. His research focuses on advanced foundation engineering. Dr. Wan leads significant research on post-grouting technology for piles, low-carbon composite piles, and pile foundation design in challenging conditions such as calcareous sands and coral reefs. He has secured substantial funding as Principal Investigator for multiple national and provincial projects, including grants from the National Natural Science Foundation of China and the Jiangsu Natural Science Foundation. Dr. Wan received the Jiangsu Rock Mechanics and Engineering Society Science and Technology Award (Special Prize, Rank 1, 2022).